MICROBIOLOGY

Shear flow patterns antimicrobial gradients across bacterial populations

Alexander M. Shuppara[1], Gilberto C. Padron[1], Anuradha Sharma[1], Zil Modi[2], Matthias D. Koch[2], Joseph E. Sanfilippo[1]*

Bacterial populations experience chemical gradients in nature. However, most experimental systems either ignore gradients or fail to capture gradients in mechanically relevant contexts. Here, we use microfluidic experiments and biophysical simulations to explore how host-relevant shear flow affects antimicrobial gradients across communities of the highly resistant pathogen *Pseudomonas aeruginosa*. We discover that flow patterns gradients of three chemically distinct antimicrobials: hydrogen peroxide, gentamicin, and carbenicillin. Without flow, resistant *P. aeruginosa* cells generate local gradients by neutralizing all three antimicrobials through degradation or chemical modification. As flow increases, delivery overwhelms neutralization, allowing antimicrobials to penetrate deeper into bacterial populations. By imaging single cells across long microfluidic channels, we observe that upstream cells protect downstream cells, and protection is abolished in higher flow regimes. Together, our results reveal that physical flow can promote antimicrobial effectiveness, which could inspire the incorporation of flow into the discovery, development, and implementation of antimicrobials.

INTRODUCTION

Antimicrobial resistance is a severe threat to human health (*1*). Fundamentally, there are three problems: Our supply of effective antimicrobials is dwindling (*1*), the development of antimicrobials lacks profitability (*2*), and most antimicrobials will likely succumb to resistance. As obvious solutions to antimicrobial resistance are not emerging, creative ideas are required. One potential idea is to focus more on how antimicrobials are delivered to target host microenvironments (*3*, *4*). During treatment, antimicrobials often fail to access the entire target population, leaving a subpopulation of cells shielded from inhibition. While antimicrobial gradients are a fundamental feature of targeted bacterial populations, it is largely unknown how the mechanical environment shapes antimicrobial gradients.

Mechanical features of the environment determine bacterial behavior and survival (*5*–*9*). In recent years, surface association and shear flow have been shown to affect a wide range of bacterial processes, such as adhesion (*10*–*13*), motility (*14*–*16*), signaling (*17*–*23*), and virulence (*24*–*28*). While researchers have focused primarily on mechanical forces (*29*), it is now clear that flow-based transport has large impacts on chemical microenvironments (*17*, *18*, *30*, *31*). For example, cell-cell communication that relies on signaling molecules such as autoinducers is typically inhibited by flow, unless cells are located in the downstream portion of a population (*30*). In addition, when one species consumes a metabolic by-product of another species, flow can spatially pattern the two species in a population (*32*). Furthermore, the ability of flow to replenish chemical stressors can increase their effectiveness (*17*, *33*, *34*). However, the impact of flow on local concentrations of antimicrobials has not been emphasized.

As flow drives antimicrobial delivery and shapes chemical microenvironments, we reason that studying how flow affects antimicrobial gradients should yield useful discoveries. Specifically, we predict that flow will rapidly replenish antimicrobials, overwhelm bacterial resistance mechanisms, and shape antimicrobial gradients across bacterial populations. Here, we implement a strategy that combines biophysical simulations and microfluidic experiments to study how antimicrobials are delivered by flow into bacterial populations. Our work connects the growing problem of antimicrobial resistance to the emerging field of mechanomicrobiology and reveals how flow can pattern bacterial populations by boosting antimicrobial delivery.

RESULTS

Shear flow patterns H_2O_2 concentration gradients across bacterial populations

To learn how flow affects antimicrobial delivery, we examined how the host-generated antimicrobial hydrogen peroxide (H_2O_2) (*35*) is delivered into populations of *Pseudomonas aeruginosa*. *P. aeruginosa* is resistant to H_2O_2 through multiple catalases and peroxidases (*17*, *36*). Using custom-fabricated 1-m-long microfluidic channels (fig. S1), we aimed to gain a spatial understanding of H_2O_2 delivery (Fig. 1A). To guide our experimental design, we first simulated the effect of flow on H_2O_2 delivery. Our simulations included three key parameters: flow, H_2O_2 diffusion, and H_2O_2 removal by cells. By holding diffusion and removal constant, we learned how increasing flow promotes delivery deeper in the simulated resistant population (Fig. 1B). In addition, by holding diffusion and flow constant, we learned how increasing removal restricts delivery into the population (fig. S2). These simulations support our model that flow patterns H_2O_2 gradients and generate testable hypotheses regarding the interaction between flow and H_2O_2 concentration.

To experimentally test how flow affects H_2O_2 gradients, we used our H_2O_2-sensitive *fro* reporter strain. Previous work established that *fro* reporter activity increases proportionately to H_2O_2 concentration and, thus, the *fro* reporter can function as a H_2O_2 biosensor. To improve our tracking of biosensor cells, we used a Δ*pilA* mutant version that is unable to move on surfaces but retains indistinguishable H_2O_2 sensitivity (Fig. 1C and fig. S3) (*18*). We seeded our 1-m–long microfluidic channel with *fro* reporter cells and subjected

[1]Department of Biochemistry, University of Illinois at Urbana-Champaign, Urbana, IL 61801, USA. [2]Department of Biology, Texas A&M University, College Station, TX 77843, USA.
*Corresponding author. Email: josephes@illinois.edu

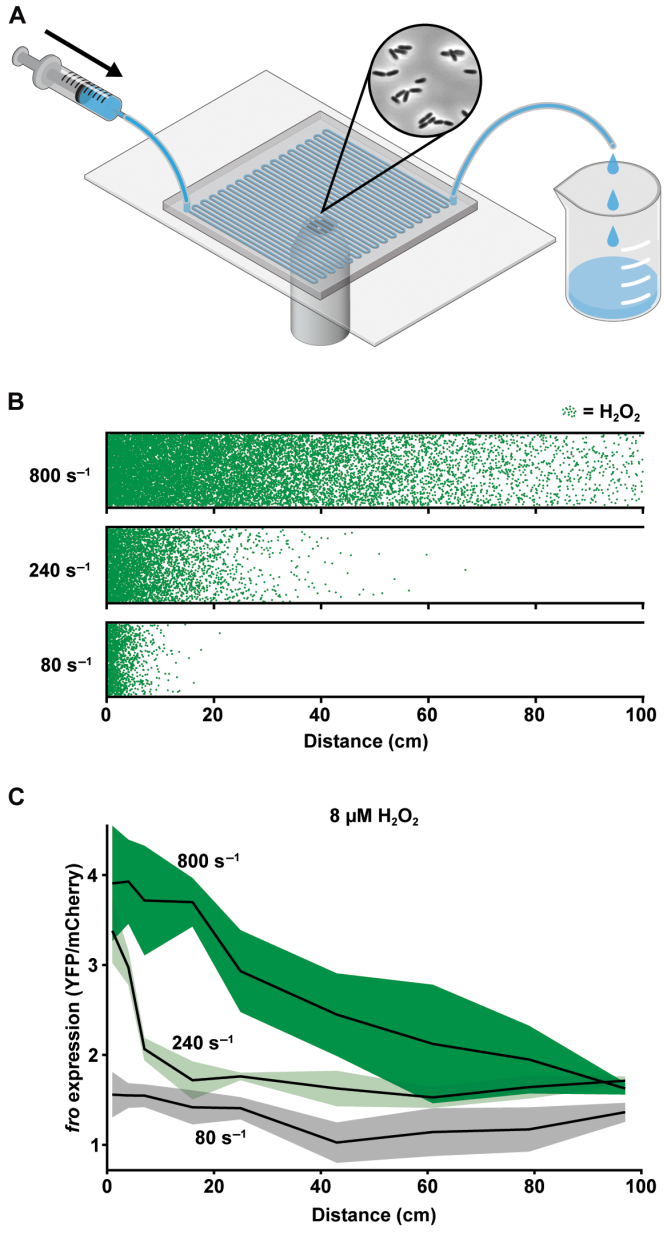

Fig. 1. Shear flow patterns H_2O_2 concentration gradients across bacterial populations. (**A**) Illustration of the microfluidic setup that allows for spatial analysis of bacterial populations. Channels are 50 μm tall, 500 μm wide, and 100 cm long. Bacteria adhere naturally to the glass surface. Flow was generated with a syringe pump, and images were taken at various distances across the channel. (**B**) Simulation of H_2O_2 molecules delivered at different flow intensities (shown as shear rates) in simulated microfluidic devices after 3 hours. Green dots represent individual H_2O_2 molecules that experienced diffusion, flow from left to right, and removal when they hit the bottom of the channel to represent bacterial removal. (**C**) *P. aeruginosa fro* reporter expression (which serves as a H_2O_2 biosensor) after 3 hours at different shear rates with LB media containing 8 μM H_2O_2 in a microfluidic channel. The *fro* experiments in (C) closely matched the biophysical simulations in (B). Shaded regions show SD of three biological replicates.

those cells to 8 μM H_2O_2. For these experiments, we used a syringe pump to deliver H_2O_2 at varied shear rates (80, 240, and 800 s^{-1}) that are commonly found in the human body (*37*). Consistent with our simulations, our experimental results show that increasing shear rate increased *fro* reporter activity and lengthened H_2O_2 spatial gradients throughout the channel (Fig. 1C and fig. S4). In further support of our simulations, increasing cell density shortened H_2O_2 spatial gradients throughout the channel (fig. S2). While increasing cell density could affect other processes, we interpreted this result to indicate that increasing total H_2O_2 removal shortened gradients. Collectively, our simulations and experiments establish that flow patterns H_2O_2 concentration gradients across resistant populations of *P. aeruginosa*.

P. aeruginosa cells are more sensitive to H_2O_2 and gentamicin in flow

How does flow affect bacterial resistance to H_2O_2? As H_2O_2 resistance relies on chemical degradation through catalases and peroxidases (fig. S5) (*38*), we reasoned that increasing delivery with flow could overcome bacterial resistance. To test our hypothesis, we treated *P. aeruginosa* cells with varying H_2O_2 concentrations with and without flow. Without flow, cells were resistant to H_2O_2, as concentrations up to 64 μM had no impact on growth (Fig. 2, A and B). With flow, cells were more sensitive to H_2O_2, as concentrations as low as 8 μM affected growth and 16 μM completely blocked growth (Fig. 2, A and B). H_2O_2 acts as a bacteriostatic antimicrobial, as flowing in media without H_2O_2 can restore growth (fig. S6). Cells exposed to 16 μM H_2O_2 at 240 s^{-1} for 2 hours were inhibited, while cells exposed to 16 μM H_2O_2 at 80 s^{-1} for 6 hours grew normally (fig. S7). As growth scaled with flow and not the total dose, we conclude that flow affects H_2O_2 sensitivity independent of the total dose delivered. These results suggest that H_2O_2 in flowing host environments restricts bacteria growth, as host H_2O_2 concentrations are typically in the low micromolar range (*17*, *35*). Thus, our results reveal that flow increases sensitivity of the resistant human pathogen *P. aeruginosa* to host-relevant concentrations of H_2O_2.

Can flow overcome resistance to clinically relevant antibiotics? Gentamicin is an effective antibiotic toward *P. aeruginosa* that targets protein synthesis (*39*). Introduction of a resistance gene encoding an acetyltransferase that directly modifies gentamicin provides *P. aeruginosa* with gentamicin resistance (fig. S5) (*40*). To test how flow affects gentamicin resistance, we treated resistant *P. aeruginosa* cells with varying gentamicin concentrations with and without flow. Without flow, cells were resistant to gentamicin, showing growth at concentrations up to 200 μg/ml (Fig. 2, C and D). With flow, cells were sensitive to gentamicin, as concentrations as low as 25 μg/ml limited growth (Fig. 2, C and D). Cells exposed to gentamicin (100 μg/ml) at 240 s^{-1} for 2 hours were inhibited, while cells exposed to gentamicin (100 μg/ml) at 80 s^{-1} for 6 hours grew normally (fig. S7). As growth scaled with flow and not the total dose, we conclude that flow affects gentamicin sensitivity independent of the total dose delivered. Together, our results reveal that flow increases sensitivity toward two chemically distinct antimicrobials by replenishing molecules faster than bacteria can neutralize them.

Antimicrobial gradients are shaped by chemical concentration and molecular size

Delivery of drugs to their target microenvironment is often a rate-limiting step in therapeutic intervention (*41*). This is particularly evident when small molecules are chemically neutralized during the delivery process, such as by resistant bacteria. One potential solution to this problem is to increase the chemical concentration administered.

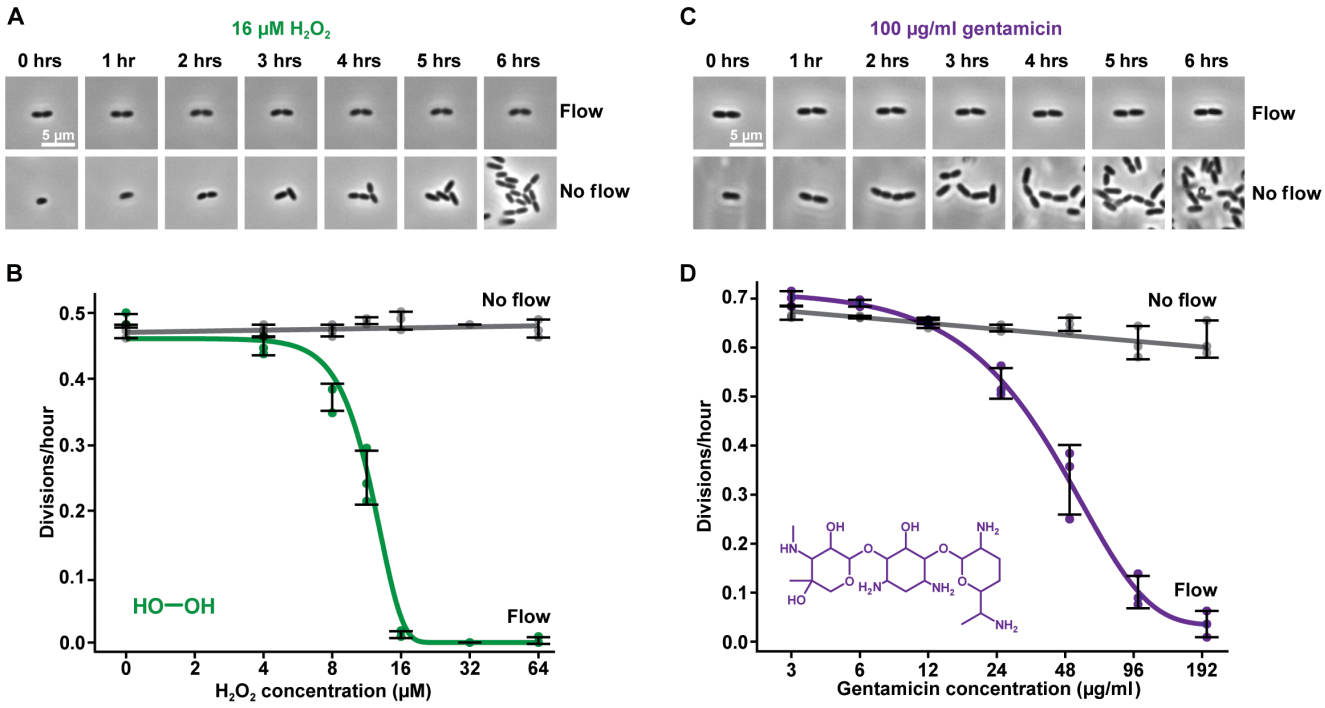

Fig. 2. *P. aeruginosa* cells are more sensitive to H_2O_2 and gentamicin in flow. (**A**) Images of naturally resistant *P. aeruginosa* cells capable of growth in 16 μM H_2O_2 over 6 hours (hrs) without flow. With flow, cells did not grow with 16 μM H_2O_2. (**B**) Growth of *P. aeruginosa* cells in M9 minimal media with flow (green) and without flow (gray) over 2 hours at various H_2O_2 concentrations. (**C**) Images of resistant *P. aeruginosa* cells capable of growth in gentamicin (100 μg/ml) over 6 hours without flow. With flow, cells did not grow with gentamicin (100 μg/ml). (**D**) Growth of *P. aeruginosa* cells in LB media with flow (purple) and without flow (gray) over 4 hours at various gentamicin concentrations. All growth experiments were performed at a shear rate of 240 s^{-1} and were imaged near the beginning of a 2-cm channel. For each biological replicate, 28 cells were chosen at random for quantification. Error bars show SD of three biological replicates.

We simulated the impact of increasing H_2O_2 concentration across a resistant *P. aeruginosa* population. Our simulations generated the hypothesis that increasing concentration allows deeper delivery into bacterial populations (Fig. 3A). While increasing concentration does not change the shape of the gradients, having more molecules at the start leads to more molecules at the end (fig. S8). Guided by our simulations, we performed growth experiments in 27-cm–long channels (fig. S1) with increasing H_2O_2 concentrations delivered with a constant flow of 240 s^{-1} (Fig. 3B). As we increased H_2O_2 from 8 to 64 μM, we observed that spatial growth gradients continually shifted downstream. These spatial growth gradients closely match our simulations and reveal that increasing concentration promotes delivery deeper into resistant *P. aeruginosa* populations.

How does the physical size of an antimicrobial affect spatial gradients? Antimicrobials come in different sizes, ranging from smaller molecules (such as H_2O_2) to larger molecules (such as gentamicin). According to the Stokes-Einstein equation, as molecular size increases, diffusion decreases. Thus, the delivery of H_2O_2 and gentamicin could differ. To predict whether physical size affects delivery, we simulated the delivery of gentamicin (Fig. 3C and fig. S9) and compared with our H_2O_2 simulations (Fig. 3A). Consistent with our hypothesis that diffusion would affect delivery, our gentamicin simulations yielded delivery curves with flatter profiles and lower slopes than our H_2O_2 simulations. By simulating molecules with a wide range of diffusion coefficients (fig. S10), we established how molecular size could affect drug delivery into cellular populations. To experimentally test how molecular size affects spatial gradients, we repeated our long channel growth experiments with constant flow and increasing gentamicin concentrations (Fig. 3D). Supporting our hypothesis, gentamicin generates growth gradients that are flatter than those found for the much smaller antimicrobial H_2O_2 (Fig. 3D). Collectively, our simulations and experiments demonstrate how chemical concentration and molecular size of antimicrobials shape spatial gradients of resistant bacterial populations.

Shear flow patterns bacterial growth by shaping antimicrobial gradients

Antimicrobial resistance often depends on the collective ability of bacterial populations to neutralize molecules. Bacteria can effectively shield one another from antimicrobials and generate spatial growth gradients. On the basis of our discovery that flow can promote delivery, we reasoned that increasing flow could overcome cell-cell shielding and restore antimicrobial effectiveness throughout the entire population. To test the impact of flow, we treated resistant *P. aeruginosa* populations in 27-cm-long channels with 16 μM H_2O_2 delivered at different shear rates (80, 240, and 800 s^{-1}) (Fig. 4A). While low flow (80 s^{-1}) did not inhibit any growth, medium flow (240 s^{-1}) generated spatial growth gradients where cells at the start of the channel shielded cells at the end of the channel (Fig. 4A). In contrast, high flow (800 s^{-1}) overwhelmed cell-cell shielding and restored the antimicrobial effectiveness of H_2O_2. Thus, our results highlight how flow can overcome population-level resistance by enhancing the physical process of delivery.

To explore whether flow can overcome population-level shielding of other antimicrobials, we replicated our experiments with gentamicin. Gentamicin is an aminoglycoside that inhibits protein

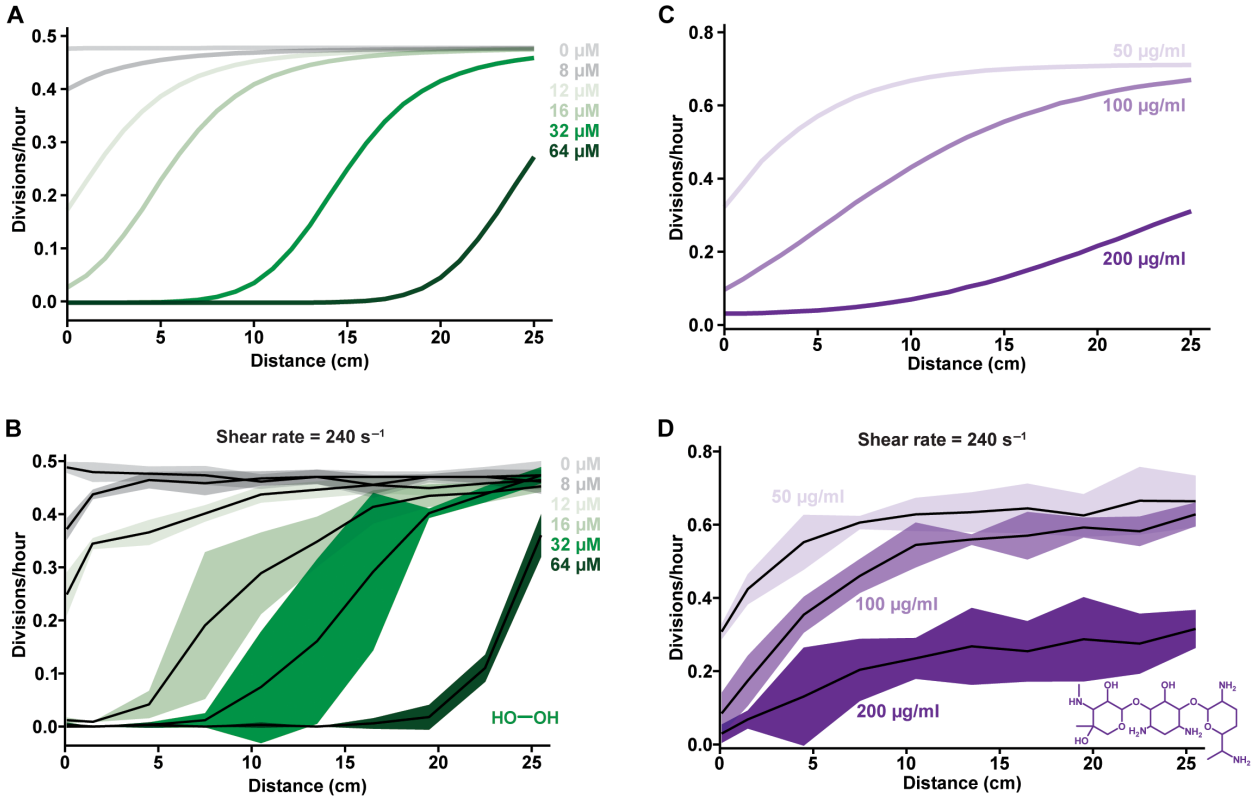

Fig. 3. Antimicrobial gradients are shaped by concentration and molecular size. (**A**) Simulations of cell growth after 2 hours across a microfluidic channel with increasing concentrations of H_2O_2 predict that growth gradients shift downstream as concentration increases. (**B**) Experiments measuring *P. aeruginosa* growth closely match the simulations in (A). Experiments were performed for 2 hours in M9 minimal media supplemented with various H_2O_2 concentrations. (**C**) Simulations of cell growth after 4 hours across a microfluidic channel with increasing concentrations of gentamicin predicts that growth gradients shift downstream as concentration increases. The predicted gradients have flatter slopes than those in (A) for H_2O_2, as gentamicin is larger and diffuses more slowly. (**D**) Experiments measuring *P. aeruginosa* growth closely match the simulations in (C). Experiments were performed for 4 hours in LB media supplemented with various gentamicin concentrations. All simulations included molecular diffusion, flow, removal, and the relationship between concentration and growth from Fig. 2. All growth experiments were performed in 27-cm–long channels at a shear rate of 240 s^{-1}. For each biological replicate, 28 cells were chosen at random for quantification. Shaded regions show SD of three biological replicates.

synthesis (*39*), and we used *P. aeruginosa* cells with an acetyltransferase that provided resistance to gentamicin (*40*). Using 27-cm-long channels, we delivered gentamicin (100 μg/ml) with varied shear rates (80, 240, and 800 s^{-1}) (Fig. 4B). Similar to H_2O_2, low flow (80 s^{-1}) did not inhibit growth, medium flow (240 s^{-1}) generated spatial growth gradients because of cell-cell shielding, and high flow (800 s^{-1}) restored the effectiveness of gentamicin throughout the entire population (Fig. 4B). These results reinforce our conclusion that flow can overcome population-level shielding and suggest that this is a broadly conserved biophysical phenomenon.

To further explore the effect of flow on antimicrobial shielding, we extended our experimental approach to the β-lactam antibiotic carbenicillin. Carbenicillin inhibits cell wall biosynthesis (*42*), and we used *P. aeruginosa* cells with a β-lactamase that provides resistance to carbenicillin (fig. S5) (*43*). Flow increases the sensitivity of cells to carbenicillin (fig. S11) such that carbenicillin (30 μg/ml) inhibits cell division and increases cell length (fig. S12). Using 27-cm-long channels, we delivered carbenicillin (30 μg/ml) (Fig. 4C) with varied shear rates (40, 80, and 800 s^{-1}). Similar to H_2O_2 and gentamicin, low flow (40 s^{-1}) did not inhibit growth, medium flow (80 s^{-1}) generated spatial growth gradients because of cell-cell shielding, and high flow (800 s^{-1}) restored the effectiveness of carbenicillin throughout the entire population (Fig. 4C). Together, our experiments with H_2O_2, gentamicin, and carbenicillin demonstrate that flow has a powerful ability to pattern spatial gradients of bacterial growth by boosting antimicrobial delivery.

DISCUSSION

Our experiments and simulations demonstrate how flow patterns gradients across bacterial populations by enhancing antimicrobial delivery. Without flow, bacteria can resist many antimicrobials through degradation or chemical modification. In low flow, resistant cells generate local zones of depletion, shield downstream cells, and generate short spatial gradients (Fig. 5A). In medium flow, the system reaches a tipping point where removal by cells and replenishment by flow occur at similar rates, leading to longer spatial gradients of concentration and growth (Fig. 5B). In high flow, delivery is faster than removal, concentration gradients do not form, and antimicrobials are effective (Fig. 5C). Thus, fast delivery by flow allows antimicrobials to penetrate deeper into target populations, preventing a subset of cells from escaping treatment (Fig. 5). Collectively, our results reveal a simple biophysical phenomenon that enhances antimicrobial effectiveness and could be

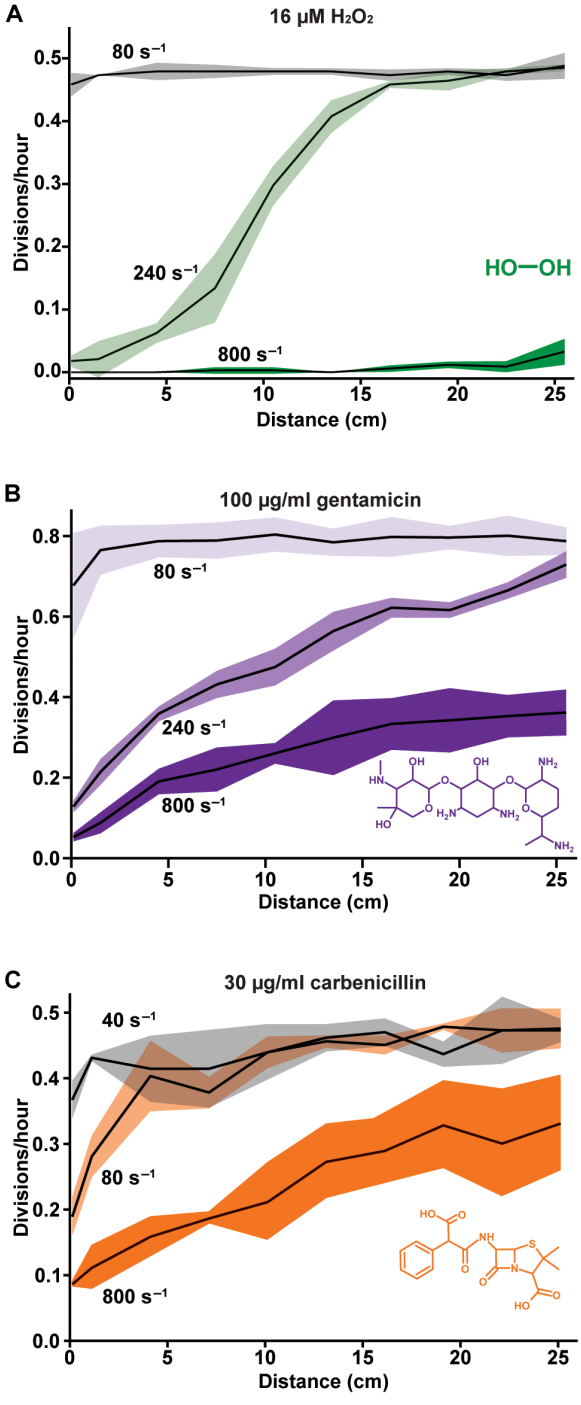

Fig. 4. Shear flow patterns bacterial growth by shaping antimicrobial gradients. (**A**) Experiments measuring *P. aeruginosa* growth for 2 hours in M9 minimal media with 16 μM H_2O_2 at various shear rates. (**B**) Experiments measuring *P. aeruginosa* growth for 4 hours in LB media with gentamicin (100 μg/ml) at various shear rates. (**C**) Experiments measuring *P. aeruginosa* growth for 4 hours in LB media with carbenicillin (30 μg/ml) at various shear rates. Higher shear rates increase the effectiveness of H_2O_2, gentamicin, and carbenicillin against resistant *P. aeruginosa* strains. We interpret that growth gradients for gentamicin and carbenicillin have flatter slopes than H_2O_2 because H_2O_2 is smaller and has a higher diffusion coefficient. All experiments were performed in 27-cm–long channels. For each biological replicate, up to 30 cells were chosen at random for quantification. Shaded regions show SD of three biological replicates.

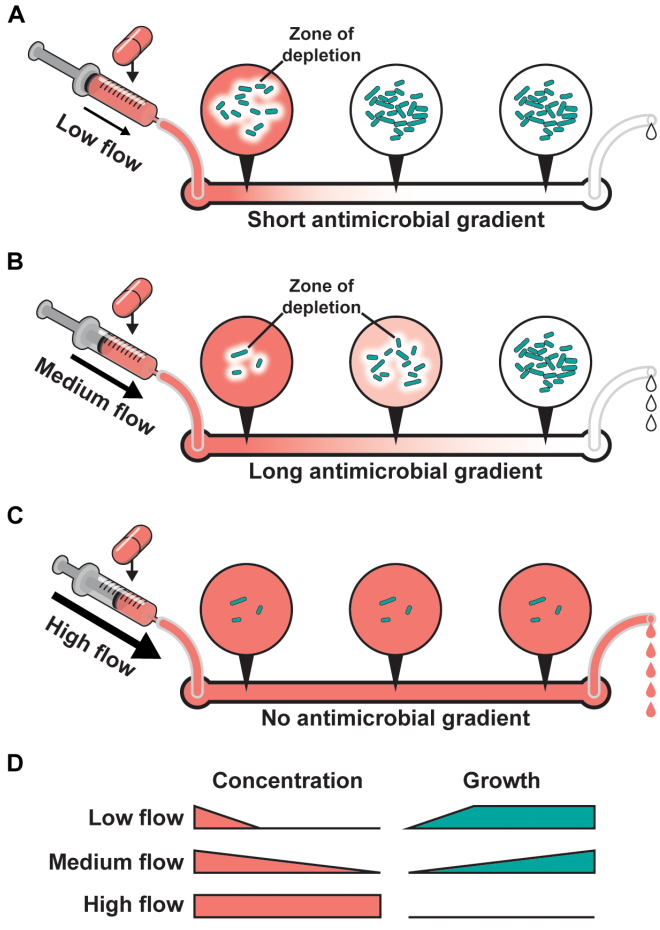

Fig. 5. Shear flow patterns antimicrobial gradients and bacterial populations. (**A**) In low flow, cell populations remove antimicrobials faster than delivery, allowing for growth and shielding downstream cells. (**B**) In medium flow, the delivery rate is similar to the removal rate, allowing antimicrobials to penetrate deeper into populations. Upstream growth is inhibited, but downstream cells can still grow. (**C**) In high flow, the delivery rate exceeds the removal rate, allowing antimicrobials to penetrate the entire population. Thus, high flow blocks the growth of the entire resistant population. (**D**) Increasing flow patterns antimicrobial gradients, which then pattern bacterial growth gradients.

leveraged to revitalize antimicrobials that appear neutralized by bacterial resistance.

How generalizable is the phenomenon that flow shapes antimicrobial gradients? As our experiments have been performed with three chemically distinct antimicrobials (H_2O_2, gentamicin, and carbenicillin), we conclude that the ability of flow to pattern antimicrobials is widely relevant. We have shown that flow can enhance the effectiveness of two clinically important antibiotic classes: aminoglycosides (represented by gentamicin) and β-lactams (represented by carbenicillin). As gentamicin is modified via a cellular acetylase (*40*) and carbenicillin is broken apart by a cellular β-lactamase (fig. S6) (*42*), flow can overcome different mechanisms of resistance. On the basis of our model, resistance mechanisms that decrease antimicrobial concentration should be affected by flow, while resistance mechanisms that do not affect concentration (such as modification of the target site) may not be affected by flow. Also, the ability of flow to shape antimicrobial gradients does not depend on attributes

exclusive to *P. aeruginosa*, indicating that flow should have similar impacts on populations of other bacterial species. Consequently, for any antimicrobial that is chemically destroyed or modified by resistant bacteria, it is logical to infer that flow has an important role in shaping antimicrobial gradients across target populations.

How does flow increase antimicrobial effectiveness and shape gradients? Our results show that the relationship between delivery with flow and removal by cells can determine antimicrobial effectiveness. Our results demonstrate that shear rate and antimicrobial concentration affect spatial gradients independent of the total dosage administered (fig. S13). As an analogy, we compare our results to the concept of alcohol consumption in humans. When humans consume alcohol, the total amount is often less important than the rate of consumption. For example, drinking 10 alcohol equivalents in 10 hours may have negligible effects, while drinking 10 alcohol equivalents in 1 hour will have extreme negative effects. In our study, we identified a parallel situation where the rate at which antimicrobials are delivered determines the magnitude of their effect.

How could increasing flow improve antimicrobial treatments? Now, it is assumed that host flow will deliver oral and intravenous antimicrobials to their target environment. However, antimicrobial treatments often fail when the entire target population is not inhibited. In addition, fears of resistance or persistence increase when a bacterial subpopulation escapes treatment. Thus, it is a great challenge to understand how flow-based delivery modulates antimicrobial effectiveness. The results we present here suggest that flow can increase delivery, abolish protective gradients, and increase antimicrobial effectiveness. We make the notable observation that increasing concentration and increasing flow have very similar impacts on bacterial populations. While it is widely accepted that increasing concentration will increase effectiveness, the idea of increasing flow has not been explored. Our results lead to the tempting idea that increasing flow during antimicrobial treatment could improve patient outcomes. At this point, it is unclear how increasing flow would be implemented safely in a clinical setting. However, we are cautiously optimistic that the fundamental discovery we present here could inspire innovative approaches that leverage flow as a strategy to increase antimicrobial effectiveness.

Clinical measurements of bacterial antibiotic susceptibility are performed without flow. Our results reveal that the absence of flow could misrepresent bacterial susceptibility. We have shown that the human pathogen *P. aeruginosa* can appear resistant to antimicrobials in diagnostic assays without flow while retaining sensitivity to antimicrobials in assays with flow. Our results provide a proof of principle that measuring bacterial resistance in static cultures can underestimate antimicrobial effectiveness under host-relevant conditions. In addition, our work reveals that even when dosage is held constant, drug effectiveness can be enhanced simply by increasing flow. Thus, we argue that there is a great opportunity to improve bacterial diagnostics through the incorporation of flow and propose that fine-tuning flow could represent a physical strategy to combat antimicrobial resistance.

METHODS

Bacterial strains and growth conditions

P. aeruginosa PA14 and mutant strains used in this paper are described in table S1. *P. aeruginosa* cultures were grown in either LB broth or M9 minimal medium on a cell culture roller drum and on LB plates (1.5% Bacto Agar) at 37°C. LB broth was prepared using LB broth Miller (BD Biosciences). M9 minimal medium was prepared as 1× M9 salts, 0.4% glucose, 2 mM $MgSO_4$, and 100 μM $CaCl_2$.

Preparation of antimicrobial solutions

LB with H_2O_2 was generated as previously described (*17*). Briefly, LB was conditioned to remove endogenous H_2O_2 and then defined concentrations of H_2O_2 were added back. Conditioning was done by diluting *P. aeruginosa* from an overnight culture into LB at a 1:100 ratio, incubating for 1 hour at 22°C, and filtering to remove cells. H_2O_2 solutions were prepared from a 30% (w/w) stock solution (Sigma-Aldrich). Gentamicin stock solutions were prepared from gentamicin sulfate (VWR) dissolved in water. Carbenicillin stock solutions were prepared from carbenicillin disodium salt (Gold Biotechnology) dissolved in water.

Fabrication of microfluidic devices

Microfluidic devices were prepared as previously described (*17*). Briefly, photomasks were designed on Illustrator (Adobe Creative Suite) and printed by Artnet Pro Inc. Using soft lithography techniques, photomask patterns were transferred onto 100-mm silicon wafers (University Wafer) that were spin coated with SU-8 3050 photoresist (MicroChem). Microfluidic devices are made of polydimethylsiloxane (Dow SYLGARD 184 Kit) at a 1:10 ratio and are plasma treated to bond on a superslip micro cover glass (60 mm by 35 mm by 0.16 mm; Ted Pella Inc.). Growth experiments used channels with dimensions of 500 μm wide by 50 μm tall by 2 cm long or 500 μm wide by 50 μm tall by 27 cm long with eight turns. *fro* reporter experiments used channels with dimensions of 500 μm wide by 50 μm tall by 100 cm long with 32 turns.

Phase contrast and fluorescence microscopy

Time-lapse images were captured on a Nikon ECLIPSE Ti2-E inverted microscope using the NIS Elements interface. For all imaging, we used a Nikon 40× Plan Ph2 0.95–numerical aperture objective, a Hamamatsu ORCA-Flash 4.0 LT3 Digital complementary metal-oxide semiconductor camera, and a Lumencor SOLA Light Engine light-emitting diode light source.

Preparation of microfluidic devices with bacteria

Microfluidic devices were loaded with bacteria as previously described (*17*). Briefly, all experiments were performed at ~22°C and with midlog bacterial cultures. Cultures were loaded into microfluidic devices via a syringe (BD Biosciences) on a syringe pump (KD Scientific Legato 210) set at 10 μl/min. Cells were allowed to adhere for 10 min before experimental flow exposure. For experiments changing population density, midlog bacterial cultures were either diluted or concentrated 10-fold in LB media before loading into microfluidic devices. Device inlets are attached to a length of polyethylene tubing [0.015″ (inner diameter) by 0.043″ (outer diameter); Brain Tree Scientific] that is sheathed over a hypodermic needle (26-gauge by 1/2″; Air-Tite Products) that is affixed on a syringe. Device outlets contain another length of tubing for vacating spent media into a bleach-containing waste container. Medium-filled syringes were fastened on a syringe pump that was set at flow rates between 0.5 and 10 μl/min, which corresponds with shear rates between 40 and 800 s^{-1}.

Shear rate calculations

The shear rate experienced in microfluidic devices was calculated using this equation

$$\frac{6Q}{wh^2}$$

where Q is the flow rate, w is the channel width, and h is the channel height. The shear rate is specified throughout in units of s^{-1}.

Quantification of *fro* expression

Expression of *fro* reporter activity was quantified as previously described (*17*). Briefly, images were captured every 30 min for 4 hours. Quantification used a MATLAB (MathWorks)–based program to identify and quantify single-cell fluorescence intensity. Yellow fluorescent protein fluorescence was used to quantify *fro* expression, and mCherry fluorescence was used as a normalization control. Reporter strains expressed mCherry from a chromosomally encoded constitutive promoter ($P_{A1/04/03}$) (*18*). *fro* reporter activity was quantified as the ratio of yellow fluorescent protein to mCherry. Experiments measuring *fro* expression used wild-type reporter cells (JS16) or Δ*pilA* mutant reporter cells (JS27).

Quantification of cellular growth

To measure cell growth during antimicrobial treatments with and without flow, images were captured every 5 min for up to 6 hours. Cell growth quantification was performed manually on ImageJ software by counting total divisions and dividing by time. At least 28 cells per field were chosen at random for growth tracking. All growth experiments were performed with cells lacking *pilA*, which prevented twitching motility and allowed for easy cell tracking. H_2O_2 and carbenicillin growth experiments used strain JS176, which contained an unmarked Δ*pilA*::FRT mutation. Gentamicin growth experiments used strain JS177, which contained a Δ*pilA*::*aacC1* mutation that provided resistance to gentamicin. H_2O_2 growth experiments were performed in M9 media with glucose. Gentamicin and carbenicillin growth experiments were performed in LB media.

Biophysical simulations

Simulations of molecular advection and diffusion were performed as previously described (*17*). Briefly, simulated channels were randomly filled with molecules that were assigned diffusive behavior by combining laminar transport and Brownian dynamic simulations. Channel parabolic flow speed profiles were modeled using the Hagen-Poiseuille equation. Molecules were allowed to diffuse along the x axis and y axis of the channel. H_2O_2 was simulated with a diffusion coefficient of 1.5×10^{-9} m^2/s. Molecular removal was estimated to be 1 of every 100 molecules that reached the channel bottom (where cells are located). Gentamicin simulations were performed using flow and removal parameters matching the H_2O_2 simulations. The diffusion coefficient used for gentamicin was 1.5×10^{-10} m^2/s, which is 10-fold less than H_2O_2, accounting for the molar mass of gentamicin being ~10-fold greater than H_2O_2. Growth simulations were generated by combining concentration simulations with the quantitative relationships between concentration and growth established in Fig. 2.

Supplementary Materials

This PDF file includes:

Figs. S1 to S13
Table S1
References

REFERENCES AND NOTES

1. Antimicrobial Resistance Collaborators, Global burden of bacterial antimicrobial resistance in 2019: a systematic analysis. *Lancet* **399**, 629–655 (2022).
2. K. H. Luepke, K. J. Suda, H. Boucher, R. L. Russo, M. W. Bonney, T. D. Hunt, J. F. Mohr III, Past, present, and future of antibacterial economics: Increasing bacterial resistance, limited antibiotic pipeline, and societal implications. *Pharmacotherapy* **37**, 71–84 (2017).
3. T. Bjarnsholt, M. Whiteley, K. P. Rumbaugh, P. S. Stewart, P. Ø. Jensen, N. Frimodt-Møller, The importance of understanding the infectious microenvironment. *Lancet Infect. Dis.* **22**, e88–e92 (2022).
4. J. Sollier, M. Basler, P. Broz, P. S. Dittrich, K. Drescher, A. Egli, A. Harms, A. Hierlemann, S. Hiller, C. G. King, J. D. McKinney, J. Moran-Gilad, R. A. Neher, M. G. P. Page, S. Panke, A. Persat, P. Picotti, K. M. Rentsch, P. Rivera-Fuentes, U. Sauer, D. Stolz, S. Tschudin-Sutter, C. Van Delden, E. Van Nimwegen, J.-W. Veening, M. Zampieri, A. S. Zinkernagel, N. Khanna, D. Bumann, U. Jenal, C. Dehio, Revitalizing antibiotic discovery and development through in vitro modelling of in-patient conditions. *Nat. Microbiol.* **9**, 1–3 (2024).
5. Y. F. Dufrêne, A. Persat, Mechanomicrobiology: How bacteria sense and respond to forces. *Nat. Rev. Microbiol.* **18**, 227–240 (2020).
6. A. Persat, C. D. Nadell, M. K. Kim, F. Ingremeau, A. Siryaporn, K. Drescher, N. S. Wingreen, B. L. Bassler, Z. Gitai, H. A. Stone, The mechanical world of bacteria. *Cell* **161**, 988–997 (2015).
7. G. C. Padron, A. M. Shuppara, J.-J. S. Palalay, A. Sharma, J. E. Sanfilippo, Bacteria in fluid flow. *J. Bacteriol.* **205**, e00400-22 (2023).
8. B.-J. Laventie, U. Jenal, Surface sensing and adaptation in bacteria. *Annu. Rev. Microbiol.* **74**, 735–760 (2020).
9. J. D. Wheeler, E. Secchi, R. Rusconi, R. Stocker, Not just going with the flow: The effects of fluid flow on bacteria and plankton. *Annu. Rev. Cell Dev. Biol.* **35**, 213–237 (2019).
10. J.-J. S. Palalay, A. N. Simsek, J. L. Reed, M. D. Koch, B. Sabass, J. E. Sanfilippo, Shear force enhances adhesion of *Pseudomonas aeruginosa* by counteracting pilus-driven surface departure. *Proc. Natl. Acad. Sci. U.S.A.* **120**, e2307718120 (2023).
11. C. K. Ellison, J. Kan, R. S. Dillard, D. T. Kysela, A. Ducret, C. Berne, C. M. Hampton, Z. Ke, E. R. Wright, N. Biais, A. B. Dalia, Y. V. Brun, Obstruction of pilus retraction stimulates bacterial surface sensing. *Science* **358**, 535–538 (2017).
12. S. Lecuyer, R. Rusconi, Y. Shen, A. Forsyth, H. Vlamakis, R. Kolter, H. A. Stone, Shear stress increases the residence time of adhesion of *Pseudomonas aeruginosa*. *Biophys. J.* **100**, 341–350 (2011).
13. E. Secchi, A. Vitale, G. L. Miño, V. Kantsler, L. Eberl, R. Rusconi, R. Stocker, The effect of flow on swimming bacteria controls the initial colonization of curved surfaces. *Nat. Commun.* **11**, 2851 (2020).
14. A. Siryaporn, M. K. Kim, Y. Shen, H. A. Stone, Z. Gitai, Colonization, competition, and dispersal of pathogens in fluid flow networks. *Curr. Biol.* **25**, 1201–1207 (2015).
15. Y. Shen, A. Siryaporn, S. Lecuyer, Z. Gitai, H. A. Stone, Flow directs surface-attached bacteria to twitch upstream. *Biophys. J.* **103**, 146–151 (2012).
16. L. Talà, A. Fineberg, P. Kukura, A. Persat, *Pseudomonas aeruginosa* orchestrates twitching motility by sequential control of type IV pili movements. *Nat. Microbiol.* **4**, 774–780 (2019).
17. G. C. Padron, A. M. Shuppara, A. Sharma, M. D. Koch, J.-J. S. Palalay, J. N. Radin, T. E. Kehl-Fie, J. A. Imlay, J. E. Sanfilippo, Shear rate sensitizes bacterial pathogens to H_2O_2 stress. *Proc. Natl. Acad. Sci. U.S.A.* **120**, e2216774120 (2023).
18. J. E. Sanfilippo, A. Lorestani, M. D. Koch, B. P. Bratton, A. Siryaporn, H. A. Stone, Z. Gitai, Microfluidic-based transcriptomics reveal force-independent bacterial rheosensing. *Nat. Microbiol.* **4**, 1274–1281 (2019).
19. M. D. Koch, C. Fei, N. S. Wingreen, J. W. Shaevitz, Z. Gitai, Competitive binding of independent extension and retraction motors explains the quantitative dynamics of type IV pili. *Proc. Natl. Acad. Sci. U.S.A.* **118**, e2014926118 (2021).
20. L. O'Neal, C. Baraquet, Z. Suo, J. E. Dreifus, Y. Peng, T. L. Raivio, D. J. Wozniak, C. S. Harwood, M. R. Parsek, The Wsp system of *Pseudomonas aeruginosa* links surface sensing and cell envelope stress. *Proc. Natl. Acad. Sci. U.S.A.* **119**, e2117633119 (2022).
21. C. J. Geiger, G. A. O'Toole, Evidence for the type IV pilus retraction motor PilT as a component of the surface sensing system in *Pseudomonas aeruginosa*. *J. Bacteriol.* **205**, e00179-23 (2023).
22. D. M. Hershey, Integrated control of surface adaptation by the bacterial flagellum. *Curr. Opin. Microbiol.* **61**, 1–7 (2021).
23. I. Hug, S. Deshpande, K. S. Sprecher, T. Pfohl, U. Jenal, Second messenger-mediated tactile response by a bacterial rotary motor. *Science* **358**, 531–534 (2017).
24. M. D. Koch, M. E. Black, E. Han, J. W. Shaevitz, Z. Gitai, *Pseudomonas aeruginosa* distinguishes surfaces by stiffness using retraction of type IV pili. *Proc. Natl. Acad. Sci. U.S.A.* **119**, e2119434119 (2022).
25. B.-J. Laventie, M. Sangermani, F. Estermann, P. Manfredi, R. Planes, I. Hug, T. Jaeger, E. Meunier, P. Broz, U. Jenal, A surface-induced asymmetric program promotes tissue colonization by *Pseudomonas aeruginosa*. *Cell Host Microbe* **25**, 140–152.e6 (2019).

26. G. Alsharif, S. Ahmad, M. S. Islam, R. Shah, S. J. Busby, A. M. Krachler, Host attachment and fluid shear are integrated into a mechanical signal regulating virulence in *Escherichia coli* O157:H7. *Proc. Natl. Acad. Sci. U.S.A.* **112**, 5503–5508 (2015).
27. A. Persat, Y. F. Inclan, J. N. Engel, H. A. Stone, Z. Gitai, Type IV pili mechanochemically regulate virulence factors in *Pseudomonas aeruginosa*. *Proc. Natl. Acad. Sci. U.S.A.* **112**, 7563–7568 (2015).
28. A. Siryaporn, S. L. Kuchma, G. A. O'Toole, Z. Gitai, Surface attachment induces *Pseudomonas aeruginosa* virulence. *Proc. Natl. Acad. Sci. U.S.A.* **111**, 16860–16865 (2014).
29. R. Chawla, R. Gupta, T. P. Lele, P. P. Lele, A skeptic's guide to bacterial mechanosensing. *J. Mol. Biol.* **432**, 523–533 (2020).
30. M. K. Kim, F. Ingremeau, A. Zhao, B. L. Bassler, H. A. Stone, Local and global consequences of flow on bacterial quorum sensing. *Nat. Microbiol.* **1**, 15005 (2016).
31. J. Nguyen, V. Fernandez, S. Pontrelli, U. Sauer, M. Ackermann, R. Stocker, A distinct growth physiology enhances bacterial growth under rapid nutrient fluctuations. *Nat. Commun.* **12**, 3662 (2021).
32. J. P. H. Wong, M. Fischer-Stettler, S. C. Zeeman, T. J. Battin, A. Persat, Fluid flow structures gut microbiota biofilm communities by distributing public goods. *Proc. Natl. Acad. Sci. U.S.A.* **120**, e2217577120 (2023).
33. V. Lagage, V. Chen, S. Uphoff, Adaptation delay causes a burst of mutations in bacteria responding to oxidative stress. *EMBO Rep.* **24**, e55640 (2023).
34. D. Choudhary, V. Lagage, K. R. Foster, S. Uphoff, Phenotypic heterogeneity in the bacterial oxidative stress response is driven by cell-cell interactions. *Cell Rep.* **42**, 112168 (2023).
35. H. J. Forman, A. Bernardo, K. J. A. Davies, What is the concentration of hydrogen peroxide in blood and plasma? *Arch. Biochem. Biophys.* **603**, 48–53 (2016).
36. W. Panmanee, D. J. Hassett, Differential roles of OxyR-controlled antioxidant enzymes alkyl hydroperoxide reductase (AhpCF) and catalase (KatB) in the protection of *Pseudomonas aeruginosa* against hydrogen peroxide in biofilm vs. planktonic culture. *FEMS Microbiol. Lett.* **295**, 238–244 (2009).
37. K. S. Sakariassen, L. Orning, V. T. Turitto, The impact of blood shear rate on arterial thrombus formation. *Future Sci. OA* **1**, FSO30 (2015).
38. J. A. Imlay, Cellular defenses against superoxide and hydrogen peroxide. *Annu. Rev. Biochem.* **77**, 755–776 (2008).
39. M. Lang, A. Carvalho, Z. Baharoglu, D. Mazel, Aminoglycoside uptake, stress, and potentiation in Gram-negative bacteria: New therapies with old molecules. *Microbiol. Mol. Biol. Rev.* **87**, e0003622 (2023).
40. S. Magnet, J. S. Blanchard, Molecular insights into aminoglycoside action and resistance. *Chem. Rev.* **105**, 477–498 (2005).
41. J. Gao, J. M. Karp, R. Langer, N. Joshi, The future of drug delivery. *Chem. Mater. Publ. Am. Chem. Soc.* **35**, 359–363 (2023).
42. K. Bush, P. A. Bradford, Epidemiology of β-lactamase-producing pathogens. *Clin. Microbiol. Rev.* **33**, e00047 (2020).
43. S. W. Newsom, R. B. Sykes, M. H. Richmond, Detection of a β-lactamase markedly active against carbenicillin in a strain of Pseudomonas aeruginosa. *J. Bacteriol.* **101**, 1079–1080 (1970).
44. L. G. Rahme, E. J. Stevens, S. F. Wolfort, J. Shao, R. G. Tompkins, F. M. Ausubel, Common virulence factors for bacterial pathogenicity in plants and animals. *Science* **268**, 1899–1902 (1995).

Acknowledgments: We thank J. Palalay, P. Sharma, N. Martin, S. Nair, J. Imlay, T. Kehl-Fie, W. van der Donk, D. Kearns, and Z. Gitai for helpful discussions and comments on the manuscript. **Funding:** This work was supported by start-up funds from the University of Illinois at Urbana-Champaign and grants K22AI151263 and R35GM155443 from the National Institutes of Health to J.E.S. **Author contributions:** A.M.S.: writing—original draft, conceptualization, investigation, writing—review and editing, methodology, resources, data curation, validation, formal analysis, and visualization. G.C.P.: conceptualization, investigation, methodology, validation, formal analysis, and visualization. A.S.: conceptualization, validation, and formal analysis. Z.M.: investigation, resources, data curation, validation, formal analysis, software, and visualization. M.D.K.: writing—original draft, investigation, methodology, resources, data curation, validation, supervision, formal analysis, software, and project administration. J.E.S.: writing—original draft, conceptualization, investigation, writing—review and editing, methodology, funding acquisition, validation, supervision, formal analysis, project administration, and visualization. **Competing interests:** The authors declare that they have no competing interests. **Data and materials availability:** All data needed to evaluate the conclusions of this paper are present in the paper and/or the Supplemental Materials.

Submitted 16 August 2024
Accepted 4 February 2025
Published 12 March 2025
10.1126/sciadv.ads5005